Int J Adv Manuf Technol (2013) 69:499–507
DOI 10.1007/s00170-013-5051-5

ORIGINAL ARTICLE

Influence of the abradant's composition on the selected physical properties in the process of front grinding of surfaces with microcrystalline sintered corundum grinding wheels

Czesław Niżankowski

Received: 20 November 2012 / Accepted: 29 April 2013 / Published online: 17 May 2013

Abstract This paper presents the results of experimental research on the influence of the composition of the abradants applied in the microcrystalline sintered corundum grinding wheels at the maximum temperature obtained in the grinding zone, maximum grinding power thrust component, grinding power feed component, active grinding power, and volumetric abradant wear. Tests were conducted in the conditions of front finishing grinding of flat surfaces of the objects made of corrosion-resistant steel, with austenitic structure. In our tests, we used a mini-grinder for flat surfaces, controlled by a CNC system, shank mounted grinding wheels made of mixed electrocorundum-cubitron abradant, a piezoelectric dynamometer, a thermal camera, a digital power analyzer, and a laser gauge. The test results were subjected to statistical and substantive analyses. It was found that, together with a proportional increase of the microcrystalline sintered corundum content in the grinding wheel's material, the values of the indicated physical properties displayed a decreasing tendency that could be determined by the trend functions, in the form of second-degree polynomials, without interaction. It was further found that such changes in the abradant composition significantly influenced the changes of the values of selected physical properties, and the test results well-approximated by the test object functions, in the form of third-degree polynomials, without interaction. The test object functions were characterized by the occurrence of local extremes whose locations indicated that it was the most beneficial to operate grinding wheels with the abradant content belonging to the range of 7CB–9CB, in the assumed testing conditions.

Keywords Grinding · Abradant composition · Temperature · Grinding power components · Grinding power · Grinding wheel's wear

1 Introduction

In 1910, Jeppson and Saunders developed a method of producing white noble electrocorundum by alumina melting in an electric-resistant arc furnace. They obtained a new abradant whose properties were considerably different from those of ordinary electrocorundum. White noble electrocorundum is primarily characterized by a higher chemical purity and a lower quantity of glassy phase in comparison to ordinary electrocorundum. Consequently, allotriomorphic grains of abradant grains have weaker bonds between each other, less glassy phase is concentrated on the grain edges, and the spaces between the grains are more open in each abradant grain [1]. Those properties allow for temperature reduction in the grinding zone and obtaining the so-called "cold grinding" effect. For that reason, white noble electrocorundum is mostly applied in the conditions of finishing machining. However, upon the material's development, it was found that the production process was unecological and required a lot of energy. In addition, the process made it impossible to produce grinding grains with required shape and dimensional proportions (Fig. 1) [2, 3].

C. Niżankowski (✉)
Department of Mechanical Engineering, Institute of Production Engineering, Cracow University of Technology, Cracow, Poland
e-mail: nizankowski@mech.pk.edu.pl

Fig. 1 A general view of abradant grains made of white noble electrocorundum 99A, grain number 60

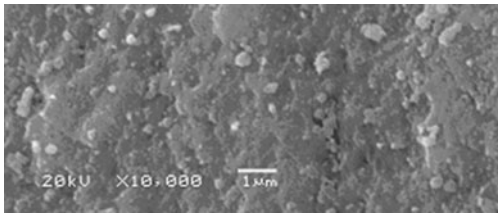

Fig. 3 Microstructure of abradant grains made of microcrystalline sintered corundum CB

Owing to that, research was implemented in the 1980s to obtain a new generation sintered corundum, manufactured under the alumina submicropowder sintering technology applied to alumina precipitated from boehmite (γ-AlOOH) by the sol–gel technology in a chemical process (Fig. 2) [4–8].

Microcrystalline sintered corundum (that is how it was called in international literature) was produced for the first time by the 3M Company in 1981 under the commercial name of CubitronTM. Presently, microcrystalline sintered corundum is manufactured by five companies based on slightly differing technologies. For that reason, particular material variations display different properties than those of CubitronTM and they are marked individually [4, 5].

The grains of microcrystalline sintered corundum (which is also sometimes called submicrocrystalline sintered corundum) are composed of strongly sintered particles, with the dimensions that are usually smaller than 1 μm (Fig. 3) [4, 8, 9].

In comparison to noble electrocorundum, the abradant grains of microcrystalline sintered corundum are characterized by larger ductility and durability as a result of self-sharpening capability on the microscale, with slightly lower microhardness at the same time. Owing to those properties, grinding wheels made of microcrystalline sintered corundum have a very wide range of industrial applications, also in the area of dry grinding or grinding in the MQL conditions [9–12].

Presently, microcrystalline sintered corundum grinding wheels are usually made of mixed abradant containing white noble electrocorundum and microcrystalline sintered corundum, in various volumetric proportions. The proportions are reflected in the abradant marking system. For example, abradant 5CB means that 50 % of the whole abradant volume is filled with microcrystalline sintered corundum (e.g., CubitronTM: for the needs of this study, we identify it by the CB abbreviation), while the remaining 50 % is filled with white noble electrocorundum 99A. Such grinding wheels are usually fabricated with ceramic binder or, recently, a glass-crystalline one (Fig. 4). Currently, the market offers only a range of grinding wheels made of microcrystalline sintered corundum composed of odd-numbered products, e.g., 1CB, 3CB, 5CB, 7CB, and 9CB. Grinding wheels with the abradant made of 100 % microcrystalline sintered corundum are produced only for special applications [4, 9, 10].

The catalogs of particular manufacturers mostly specify the general rule of the abradant's composition selection, which can be reduced to the principle that with higher hardness of the top surface of the workpiece (TSW), larger length of the machining path by a single grinding grain, and larger grinding depth, or higher relative grinding effectiveness to be obtained, we should increase the microcrystalline sintered corundum content in the grinding wheel's abradant volume [2, 9]. That rule suggests linear or monotonic dependence between the abradant content and the physical parameters [10,

Fig. 2 A general view of abradant grains made of microcrystalline sintered corundum CB, grain number 60

Fig. 4 The structure of a grinding wheel made of microcrystalline sintered corundum, abradant content 5CB

13–15] selected for the purpose of this study. This suggestion is not, however, confirmed by the operating examples specified by manufacturers. Their examples clearly indicate that intermediate abradant composition applied in the grinding wheel production often prove to be optimum for the selected grinding conditions owing to the criteria that are customarily assumed for the evaluation of the grinding wheel's grindability or its physical parameters. The purpose of the present study was to find the answers to the questions: will the increase of the microcrystalline sintered corundum content in the abradant volume significantly influence the changes of the physical parameters considered in this study and are such changes linear in the process of front finishing grinding of the surfaces of materials made of stain-resistant steel, with austenitic structure?

2 Description of experimental tests

The design of experimental tests of the front finishing surface grinding process, using microcrystalline sintered corundum grinding wheels, with various abradant composition, is presented in Fig. 5.

Input parameter description:

x_1 Percentage microcrystalline sintered corundum content in the grinding wheel's abradant (i.e., 1CB=10 %, 3CB =30 %, 5CB=50 %, 7CB=70 %, 9CB=90 % of microcrystalline sintered corundum in the abradant volume).

Output parameter description:

z_1 Maximum temperature θ_{max} in the grinding zone in Kelvin

z_2 Thrust component F_p of the grinding power in newton

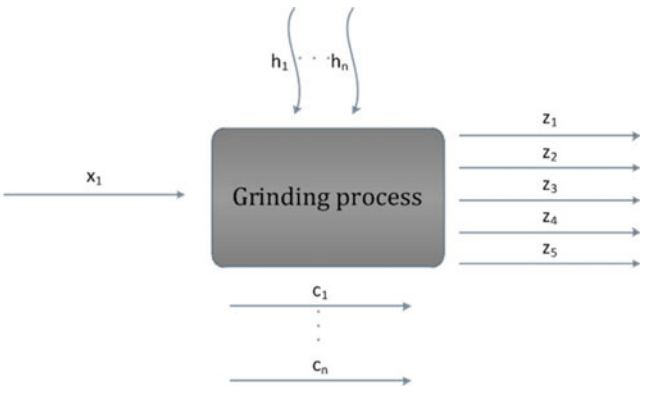

Fig. 5 Experimental test design

Fig. 6 A general view of the test bench (control unit+mini-grinder SIC330 CNC+digital power analyser DW6090+thermal camera FLIR SC620)

z_3 Feed component F_f of the grinding power in newton

z_4 Active grinding power P_c in watt

z_5 Volumetric wear of the grinding wheel V_m in cubic millimeter.

Constant factors:

c_1 Mini-grinder SIC 330 CNC (Knuth GmbH; Fig. 6)

c_2 Grinding wheel parameters: 5216 30×30×6 XX60L7V (Andre Abrasives), where XX stands for changes according to x_1 (Fig. 5)

c_3 Grinding parameters:

- Grinding velocity v_c=28.3 m/s
- Depth of cut a_e=0.002 mm
- Longitudinal feed velocity v_f=1 m/min.

c_4 Grinding method: front finishing longitudinal surface grinding, with a rectangular table grinder

c_5 Machining medium: dry grinding

c_6 Workpiece: cuboid samples, 100×24×20 mm, with preliminary machining (Ra=2±0.1 μm), steel grade 1H18N9T (vel 1.4541 EN 10088), resistant to corrosion, with austenitic structure

c_7 Grinding cycle: 3-phase, without sparking out

c_8 Truing method: diamond dresser M1020, with a 0.25-ct diamond, dressing depth a_d=0.01 mm and the cover coefficient of k_d=3

c_9 Input parameter measurement methods

c_{10} Number of machining passes: 60 leveling passes in a single grinding pass.

c_{11} Time of one machining pass of the grinding wheel: 2 s

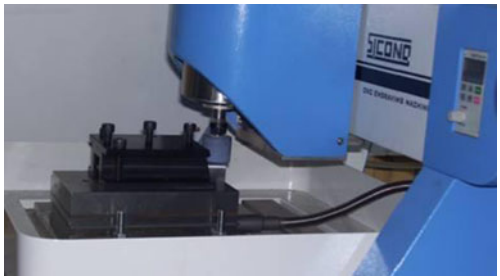

Fig. 7 The method of sample mounting in the KISTLER 9257B power meter and the form of the shank mounted grinding wheel placed in the grinder's spindle holder

Interfering factor description:

h_1 Dispersion of physical and mechanical properties of the grinding wheel
h_2 Dispersion of physical and mechanical properties of the workpiece
h_3 Inaccuracy in the performance of the assumed grinding, dressing, and other parameters.

Experimental tests were conducted in accordance with a determined complete static plan, PS/DK, treating the front finishing grinding process as five separate elementary objects. The same grinding effectiveness was applied in all the test objects. The test results for each test object took into account five values measured in five grinding cycles (five replications).

The following dependences were the test object functions: $\theta_{max}=f(XX)$, $F_p=f(XX)$, $F_f=f(XX)$, $P_c=f(XX)$, and $V_m=f(XX)$, where XX was the changing abradant composition. First, the least square method was applied to determine the trend curves for each of the samples, taking into account the functions in the form of second-degree polynomial, without interaction. Next, approximation of test results was conducted by the computer equalization method, with the functions in the form of third-degree polynomials, without interaction, and the adequacy of those functions was checked at the significance level of $\alpha=0.05$. In case of both trend curves and approximating functions, the values of determination coefficients R^2 were

Fig. 8 Basic elements of the laser gauge

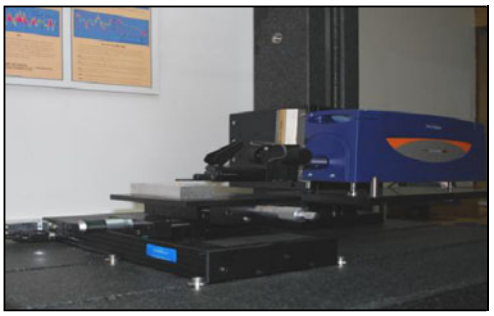

Fig. 9 Profilographometer Talysurf Form 50

calculated. The maximum temperature in the grinding zone was measured with the use of FLIR SC620 thermal camera, with the accuracy of +/− (2 % v2), operating in a set with a microcomputer equipped with ThermaCAM Researcher Pro 2.10 software. However, the measurements of active grinding power were made with the use of an NDN DW6090 digital power analyser (Fig. 6). The grinding force component measurements were made with the use of a KISTLER 9257B piezoelectric dynamometer (Fig. 7). The dynamometer was also connected to a PC, which recorded digital signals and carried out proper data processing. The measurements of the axial wear of the grinding wheel were taken with the use of a KEYENCE laser gauge (an LJ-G030 sensor and an LJ-G5001(P) controller), followed by conversion in respect of volumetric wear (Fig. 8). Regardless of the measurements specified in the input test parameter design, each time microscopic observation of the active grinding wheel surface (AGWS) was carried out and the topography of the top machined surface was checked using profilographometer TALYSURF FORM 50 from Taylor Hobson (Fig. 9). Those additional observations were carried out owing to the need of substantive evaluation of the causes of identified phenomena.

A selected thermal image of the grinding zone area, with a temperature record graph, is presented in Figs. 10 and 11. A selected printout from the power and grinding moment

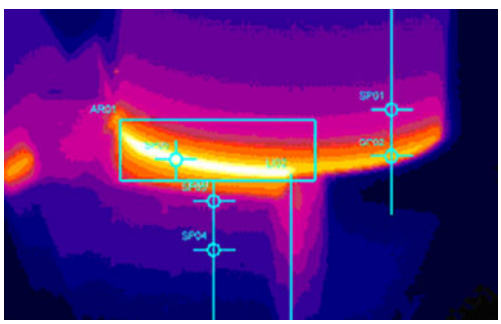

Fig. 10 IR image from the grinding zone, with marking of the measurement points and lines [16]

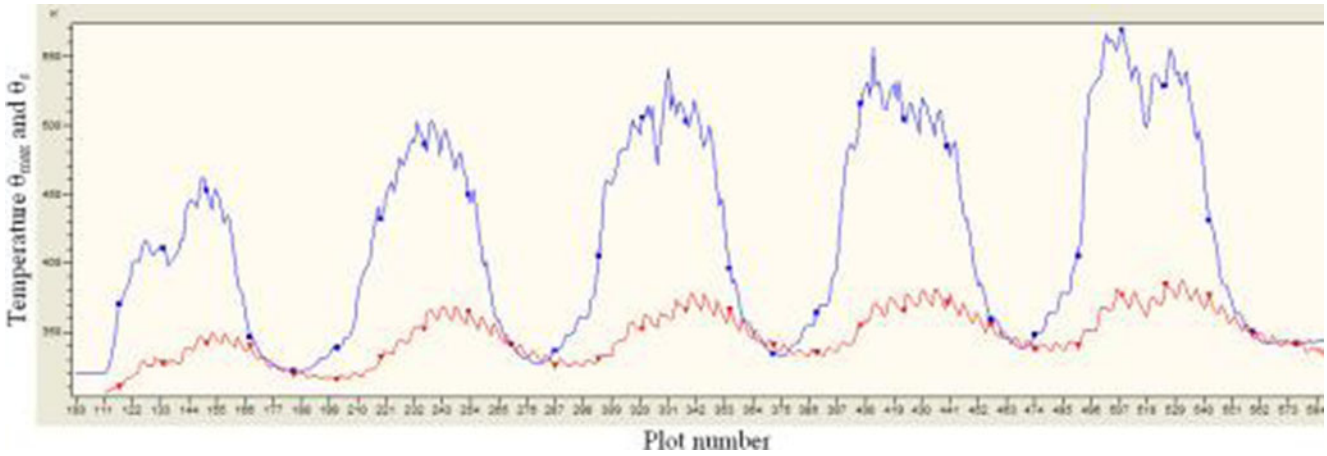

Fig. 11 Selected graph of the temperature record made during grinding with a 5216 30×30×6 5CB60L7V grinding wheel (*blue line*: θ_{max}, *red line*: θ_s—maximum temperature in the grinding wheel)

component record, in connection with the KISTLER piezoelectric dynamometer, is presented in Fig. 12.

3 Test results and statistical analysis

The experimental test results relating to the influence of the abradant composition on the selected physical parameters in the process of front finishing grinding of flat surfaces of corrosion-resistant steel, using grinding wheels made of microcrystalline sintered corundum, with various abradant compositions, are presented in Table 1.

The results were subjected to statistical analysis. In the first stage, the analyst tried to establish whether the proportions of two variances (in the systems of "u," 3CB to 1CB, 5CB to 1CB, 7CB to 1CB, and 9CB to 1CB) for the same input value of z_i would be higher than one could expect when the samples had been collected from the same population.

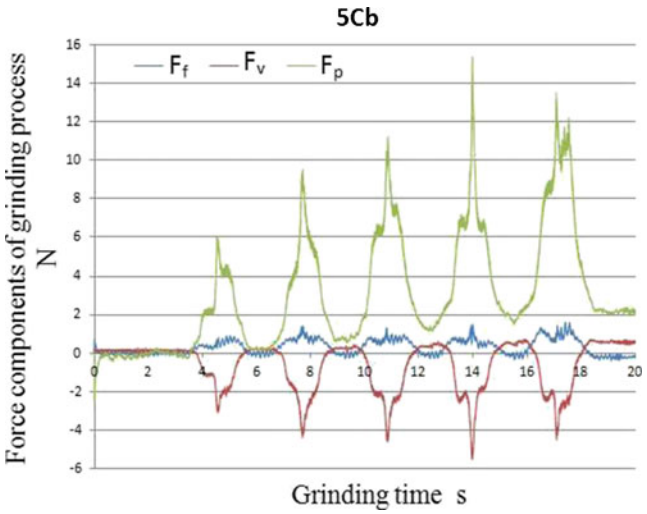

Fig. 12 Selected course of grinding force components; 5216 30×30×6 5CB60L7V grinding wheel

Zero hypotheses were set as to variance equality. To check those hypotheses, the expressions of $S^2(z_{i/u})$ were used as estimations of the variance of variables $z_{i/u}$ (based on samples), with Fisher–Snedecor statistical distribution. The results of variance analysis by test *F*, on the example of variable $z_{1/u}$, is presented in Table 2.

The comparison of the calculated values with the table values of *F* does not allow to refute zero hypotheses, with variance equality at the significance level of α=0.05. An analogous situation occurs in the cases of the remaining variables z_i. In the second stage of the statistical analysis of test results, the analyst checked whether there was a significant difference between the two average values $\bar{z}_i$ (from both test result groups, in each "u" system), for the same input value z_i. Zero hypotheses were set as to equality of respective average values in particular "u" systems. Those hypotheses were verified by the Student's *t* test, proper for checking the difference between the two average values. The results of the analysis with the test *t* of the differences between the average values, on the example of variable $z_{1/u}$, are presented in Table 3.

The comparison of calculated values of *t* with the table values of *t* allows us to state that there are significant differences between the respective average values in the particular systems "u," and the zero hypotheses are not true at the significance level of α=0.05. An analogous situation occurs in the case of the remaining variables z_i. In the third stage of the statistical analysis of

Table 1 Physical parameter test results

Abradant composition	θ_{max} (K)		F_p (N)		F_f (N)		P_c (W)		V_m (mm^3)	
	$\bar{z}_1$	S_1	$\bar{z}_2$	S_2	$\bar{z}_3$	S_3	$\bar{z}_4$	S_4	$\bar{z}_5$	S_5
1CB	646.83	57.02	27.6	8.4	7.5	3.41	405.8	2.04	0.236	0.009
3CB	810.80	33.14	35.4	9.69	10.0	4.69	502.0	1.90	0.233	0.011
5CB	526.55	39.31	11.2	3.28	1.6	0.29	266.4	4.22	0.157	0.008
7CB	468.79	41.75	13.5	3.49	0.4	0.17	248.8	4.92	0.079	0.002
9CB	549.51	70.20	12.14	3.11	1.5	0.54	263.6	3.72	0.079	0.003

$\bar{z}_i$ is the arithmetic average of the measurement results of the i-th value. S_i is the standard deviation of the measurement results of the i-th physical value

experimental test results related to the influence of the abradant content on the selected physical parameters, trend curves were designed, in the form of second-degree polynomials, for particular test objects, with the calculation of the determination coefficients R^2, followed by test result approximations by the functions in the form of third-degree polynomials, without interaction, plus determination of their adequacy at the significance coefficient of α=0.05. Since for each test object $F_{TOF} \leq F_{0.05;\ 2;\ 6}$=5.14, (where TOF=Test Object Function), there are no grounds for refutation of the hypotheses that the determined TOF values are adequate (Figs. 13, 14, 15, 16, and 17). Standard deviations of the i-th physical values are included in Table 1.

4 Merits-related tests results analysis

Even a preliminary analysis of the obtained test object functions indicates the existence of local extremes. The increase of the values of the selected physical parameters during front finishing grinding of surfaces with microcrystalline sintered corundum grinding wheels of the 1CB–3CB range is noticeable, just as the parameter minimization when machining with the grinding wheels of the 7CB–9CB range.

The TSW analysis and AGWS microscopic observations indicated that the cause of the occurrence of the maximum when grinding with a 3CB grinding wheel consisted in the appearance of the silting (gluing) process on the active grinding wheel's surface by the microchips which settled in the inter-blade spaces (Fig. 18). After those microchips were cut off from the active grinding wheel's surface, they were stuck to the workpiece's surface (Fig. 19), thus increasing the friction forces in the grinding process, and consequently causing increase of the selected physical values. The clogging of the active grinding wheel's surface results from the dominating grinding grain wear mechanism in case of 3CB abradant composition (Figs. 20 and 21). The increased friction between the grinding grains and the workpiece causes increase of the machining force value and of the grinding wheel's wear, as well as the increase of machining temperature and power (Figs. 13, 14, 15, 16, and 17). However, in case of 7CB abradant composition, the decrease of the physical values under analysis was caused by the intensification of the contribution of the grinding grain self-sharpening mechanisms to the process of grinding wheel's active surface wear (Figs. 22 and 23). The change of the dominating grain wear mechanism component resulted not only from the increase of the proportion of the Cubitron grinding grains with the self-sharpening capability in the abradant composition, but probably also from the changing minimum micromachining depth of single grinding grains, when micromachining after the traces of preceding grains (Figs. 20 and 22; Tables 4 and 5).

Table 2 Variance analysis by the test of F experimental results, in comparative studies of maximum temperature in the grinding zone

System u	$\frac{3CB}{1CB}$	$\frac{5CB}{1CB}$	$\frac{7CB}{1CB}$	$\frac{9CB}{1CB}$	Table values of F	
					$F_{0,05;4;4}$	$F_{0,1;4;4}$
Calculated values of F	2.96	2.10	1.86	1.52	6.390	4.1072

Table 3 Test t analysis of differences between the average values of comparative experimental test results of the maximum temperature θ_{max} w in the grinding zone

System u	$\frac{3CB}{1CB}$	$\frac{5CB}{1CB}$	$\frac{7CB}{1CB}$	$\frac{9CB}{1CB}$	Table values of t	
					$t_{0,05;8}$	$t_{0,1;8}$
Calculated values of t	8.59	7.02	10.66	5.63	2.306	1.860

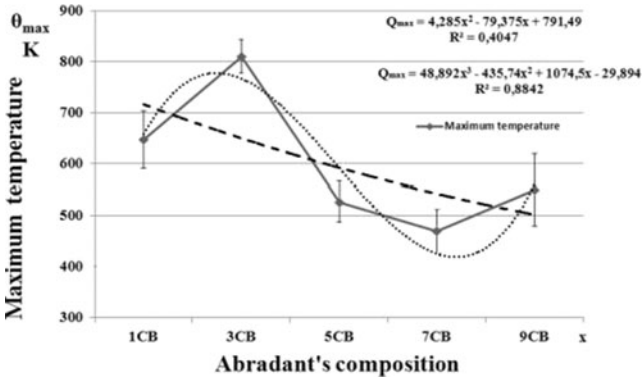

Fig. 13 The influence of microcrystalline sintered corundum abradant composition on the maximum temperature in the grinding zone

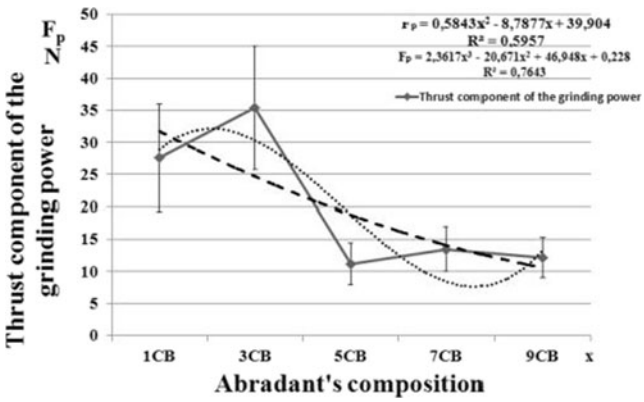

Fig. 14 The influence of microcrystalline sintered corundum abradant composition on the grinding power thrust component

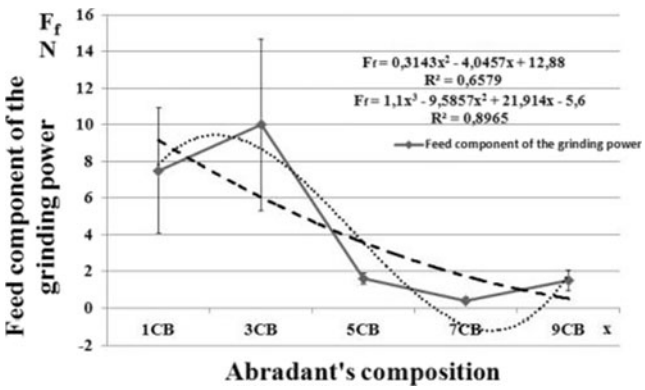

Fig. 15 The influence of microcrystalline sintered corundum abradant composition on the grinding power feed component

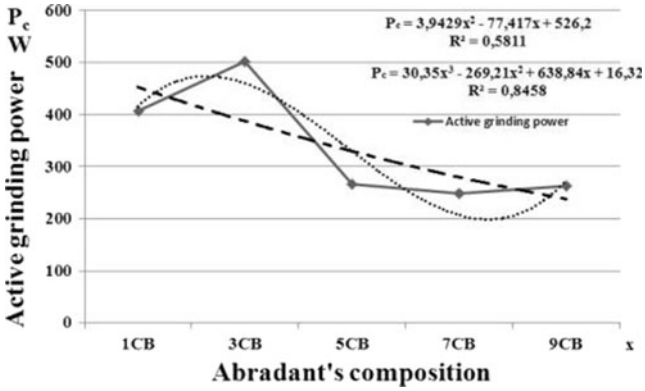

Fig. 16 The influence of microcrystalline sintered corundum abradant composition on active grinding power

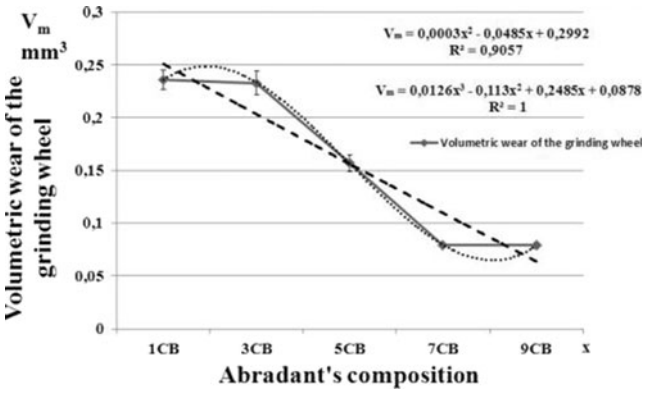

Fig. 17 The influence of microcrystalline sintered corundum abradant composition on the volumetric wear of the grinding wheel

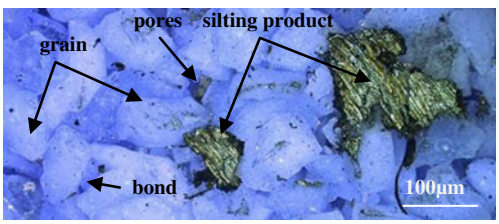

Fig. 18 A view of an active grinding wheel's surface, with the 3CB abradant composition, upon grinding completion

Fig. 19 A view of the machined surface, with a sticking chip removed from the active grinding wheel's surface

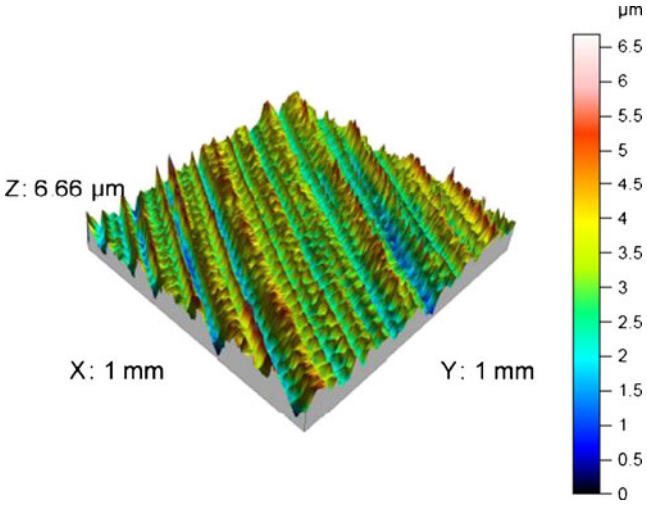

Fig. 20 Topography of the surface machined with a 3CB grinding wheel

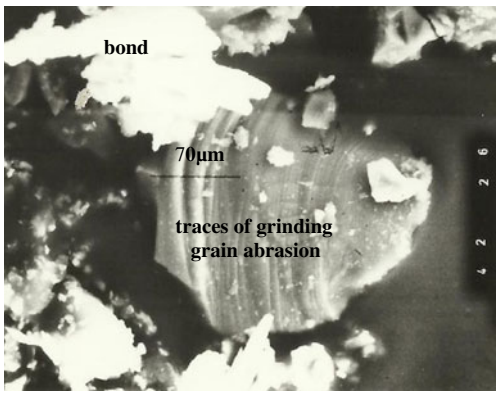

Fig. 21 A scanning image of the dominating form of grinding grain wear when machining with 3CB grinding wheels

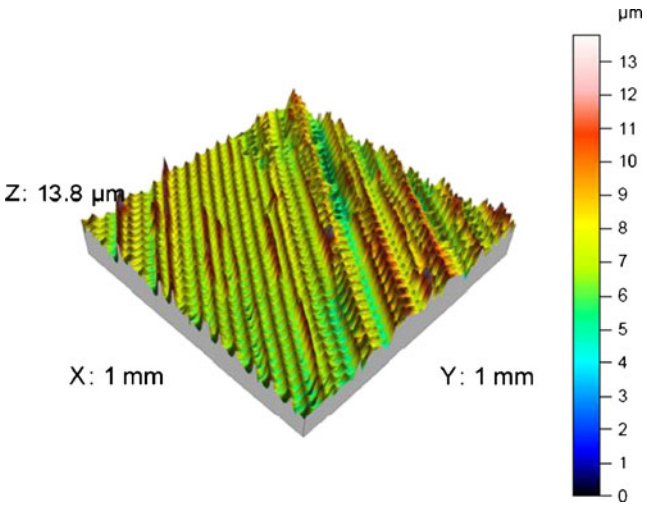

Fig. 22 Topography of the surface machined with a 7CB grinding wheel

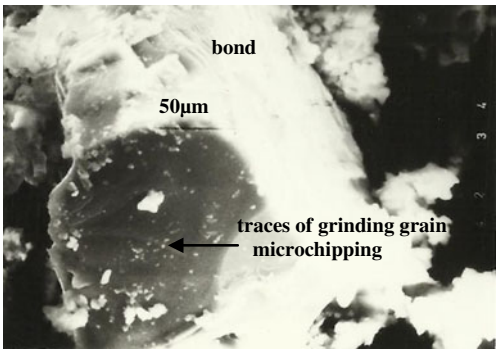

Fig. 23 A scanning image of the dominating form of grinding grain wear when machining with 3CB grinding wheels

Table 4 Height parameter values of the coarseness of the surfaces machined with 3CB grinding wheels

ISO 25178			
Height parameters			
Sq	0.711 µm	Sv	2.65 µm
Ssk	−0.262	Sz	5.52 µm
Sku	3.62	Sa	0.546 µm
Sp	2.87 µm		

Table 5 Height parameter values of the coarseness of the surfaces machined with 7CB grinding wheels

ISO 25178			
Height parameters			
Sq	1.19 µm	Sv	6.05 µm
Ssk	0.0363	Sz	11.2 µm
Sku	4.67	Sa	0.878 µm
Sp	5.2 µm		

5 Conclusions

Based on the statistically and substantively analyzed test results, it was found that, in the conditions of front finishing grinding of flat surfaces of the objects made of austenitic corrosion-resistant steel, using microcrystalline sintered corundum grinding wheels, the following regularities were found:

- The composition of the abradants of the grinding wheels used in tests indicated their significant influence (at the significance coefficient of α=0.05) on the maximum temperature in the grinding zone, thrust power component, grinding feed power, active grinding power, and volumetric grinding wheel wear.
- Together with the increase of the percentage microcrystalline sintered corundum content in the abradant, the values of the indicated physical parameters displayed a decreasing trend that could be determined by trend functions, in the form of second-degree polynomials, without interaction. That contradicted a popular industrial rule under which the respective changes have the nature of linear changes.
- The test results well-approximated the following test object functions:

– $Q_{max}=48.89\ (XX)^3-435.74(XX)^2+1{,}074.50(XX)-29.90$
– $F_p=2.36\ (XX)^3-20.67\ (XX)^2+46.95(XX)+0.23$
– $F_f=1.10(XX)^3-9.59(XX)^2+21.91(XX)-5.60$
– $P_c=30.35(XX)^3-269.21(XX)^2+638.84(XX)+16.32$
– $V_m=0.013(XX)^3-0.113(XX)^2+0.249(XX)+0.088$

Those functions indicated the existence of local extremes in the changes of the selected physical values, depending on the abradant composition changes.

- Synergic influence of the mixed 3CB abradant on the machined surface caused the occurrence of the wear phenomenon on the active grinding wheel's surface, in the form of gluing (silting), in the assumed machining conditions, which resulted from the specific properties of the ground material (in this case of low thermal conductivity of austenite, its resistance to microchip corrosion, and the adhesion capability).
- In the assumed and similar grinding conditions, it is recommended to apply the grinding wheels with the 7CB–9CB abradant content.

References

1. Woźniak (1992) Materiały Ścierne – wytwarzanie i własności. Wydawnictwo Naukowo-Techniczne, pp 97–110. Warszawa
2. Marinescu ID, Hitchiner M, Uhlmann E, Rowe WB, Inasaki I (2007) Handbook of machining with grinding wheels.CRC. Boca Raton
3. Klocke F (2009) Manufacturing processes 2: Grinding, honing, lapping. Springer-Verlag, Berlin
4. Niżankowski CZ (1996) Właściwości skrawne ściernic z korundu spiekanego. Wydawnictwo Politechniki Krakowskiej, Monografia 205, Kraków, pp 102–105
5. Heuer W (1990) Gesinteres Aluminiumoxid – ein neuer Schleistoff zum Innenrundschleifen. Wirtschaftliche Alternative. Industrie Anzeiger 112(69):44–46
6. Mayer J, Engelhorn R, Bot R, Weirich TH, Herwartz C, Klocke F (2006) Wear characteristics of second-phased-reinforced sol–gel corundum abrasives. Acta Materialia 54(13):3605–3615
7. Zi-Cheng L, Zhi-Hong L, Ai-Ju Z, Yu-Mei Z (2009) Synthesis and two-step sintering behavior of sol–gel derived nanocrystalline corundum abrasives. J Eur Ceram Soc 29:1337–1345
8. Nadolny K (2012) Wytwarzanie, właściwości zastosowanie ziaren ściernych z mikro- i submikrokrystalicznego korundu spiekanego. Mechanik 10/2012 Wydawnictwo Sigma, pp 850–857
9. Niżankowski CZ (2012) Wpływ składu ściernika na zdolność ścierną ściernic z submikrokrystalicznego korundu spiekanego. Monografia nt. Postępy w obróbce ściernej, Oficyna Wydawnicza Politechniki Wrocławskiej. Wrocław
10. Brunner G (1998) Schleifen mit mikrokristallinem Aluminiumoxid. Dr.- Ing. Dissertation, Univ, Hannover
11. Stark C (1997) Potentials of abrasive tools with microcrystalline sintered aluminium oxide. VDI-Z Integrierte Production, Issue II/97 Springer-VDI-Verlag GmbH & Co, Düsseldorf
12. Jackson MJ, Davim JP (2010) Machining with abrasives. Springer, New York
13. Lowin R (1980) Schleiftemperaturen und ihre Auswirkungen im Werkstück. Miss. RWTH, Aachen
14. Ueda T, Hosokawa A, Yamamoto A (1985) Studies on temperature of abrasive grains in grinding—application of infrared radiation pyrometer. J Eng For Industry Trans of ASME 107:127–133
15. Sherman EA, Kortel AA, Zhukovskaya AE, Nechaev YR, Azbel' YI, Shubina AE (1980) A separator for deironing sintered corundum. Refract Ind Ceram Springer-Verlag 21(9–10):522–524
16. Niżankowski Cz, Sęk K (2012) Badania porównawcze pól temperatury w procesie czołowego szlifowania płaszczyzn ściernicami z elektrokorundu szlachetnego oraz mikrokrystalicznego korundu spiekanego. The World of Machine Tools 7-9/2012, pp 18–20